Hindawi
Mathematical Problems in Engineering
Volume 2020, Article ID 8618759, 9 pages
https://doi.org/10.1155/2020/8618759

Research Article

Optimal Clutch Pressure Control in Shifting Process of Automatic Transmission for Heavy-Duty Mining Trucks

Heng Zhang,[1] **Xinxin Zhao**,[1] **and Jianning Sun**[1,2]

[1]*School of Mechanical Engineering, University of Science and Technology Beijing, Beijing 100083, China*
[2]*China Intelligent and Connected Vehicles (Beijing) Research Institute Co., Ltd, Beijing 100176, China*

Correspondence should be addressed to Heng Zhang; zhanghengustb@hotmail.com

Received 15 May 2020; Revised 6 August 2020; Accepted 18 September 2020; Published 12 October 2020

Academic Editor: Michele Guida

The optimal control of automatic transmission plays an important role in the shifting smoothness and fuel economy of heavy-duty mining trucks. In this paper, a dynamic model of the powertrain system is built to study the clutch pressure control during the shifting process. A linear-quadratic optimal regulator is used to achieve the optimum control pressure of clutches, where shifting jerk and clutch friction loss are chosen to a form quadratic performance index function. Besides, a detailed solution of the linear-quadratic problem with the disturbance matrix in the state equations is provided. This paper also carries out a software simulation and verification of the normal condition (no load without slope) and the extreme condition (full load with maximum slope). Compared with the preset reference trajectory control, the simulation results show that the proposed optimal clutch pressure control can effectively reduce jerk and friction loss during the shifting process and has good robustness to different operating conditions.

1. Introduction

Transmission is the key component of a vehicle that transmits different torque ratios at different speeds [1]. In order to make heavy-duty mining trucks face the problems of bad working conditions, poor fuel economy, and high labor intensity of drivers, AT is widely used in this field with the characteristics of strong transmission capability, smooth shifting process, and high reliability [2, 3]. In addition, under the condition of increasingly mature lockup clutch technology, the efficiency of AT has also been significantly improved [4].

In order to avoid power interruption, shift overlapping, and overheating of the clutch plate, caused by incoordination between on-coming and off-going clutches, some researchers have studied the clutch-to-clutch shifting process and divided it into four parts (preshift phase, torque phase, inertia phase, and postshift phase) [5–7]. Meng et al. [8] analyzed the AT's electrohydraulic control system and proposed a two-degree-of-freedom PID control method to optimize the duty ratio of proportional solenoid valves for the speed difference of clutch discs following a preset trajectory. Song and Sun [9] focused on the nonlinear dynamic characteristics of the wet clutch and designed a sliding mode controller to control the on-coming clutch pressure to ensure a smooth clutch-to-clutch shifting in the inertia phase. To track and control the relative speed of the clutch, eliminate the uncertainty of system parameters, and improve the robustness with respect to changing driving conditions, robust controllers, postfeedback controllers, and disturbance compensators were designed by Sanada et al. [10]. Zhao and Li [11] used the subspace identification method to describe the prediction equation of the AT powertrain system, which solved the difficulty of modeling an accurate clutch-to-clutch shifting process and then applied the model prediction controller to improve the shift quality in hardware-in-the-loop tests. Considering power, comfortability, and robustness during the clutch engagement, Wurm and Bestle [12] adopted a multiobjective genetic algorithm to achieve their balance and finally obtain Pareto optimality. In summary, since the torque signal is hard to be measured by a sensor in the torque phase, current studies mostly track a

preset reference trajectory of the on-coming clutch's relative speed for a smooth shift process in the inertial phase. However, under a wide variation of working conditions for heavy-duty mining trucks, the preset reference trajectory cannot be determined as the optimal solution of shifting jerk and clutch friction loss, which are the most important shift performance indicators.

The linear-quadratic optimal regulator (LQR) has been used in the field of vehicle powertrain system control successfully. To reduce the torsional vibration of electric vehicle transmission systems, the method of an infinite-time LQR was proposed by Lin et al. [13] to adjust the output torque of the drive motor dynamically. Gao et al. [14] used an offline finite-time LQR to track the clutch relative speed during the gear shift of an electric vehicle equipped with AMT. For the torque phase and the inertia phase of the DCT upshift process, Li and Görges [15] put forward control methods based on LQR and integral LQR, respectively, to reduce the jerk of shifting to make the vehicle shift more smoothly. However, friction loss of clutch, as another important performance index, is not considered.

Therefore, this paper proposes a linear-quadratic optimization-based clutch pressure trajectory for the shifting process of heavy-duty mining trucks equipped with AT to reduce the jerk of shifting and friction loss of clutch simultaneously. In Section 2, the dynamic modeling of powertrain systems is carried out and the AT shifting process is analyzed, followed by the design of the LQR controller for the trajectory of clutch pressure in the inertial phase (Section 3). Then, Section 4 presents the optimized results for two typical working conditions of heavy-duty mining trucks and a comparison with the preset reference trajectory. Concluding remarks are finally given in Section 5.

2. Modeling for Powertrain Systems of Heavy-Duty Mining Trucks

Equipped with automatic transmission, the powertrain system of heavy-duty mining trucks can be divided into input power module (composed of a diesel engine and a torque converter), wet clutch pressure control module, planetary gear set module, and output power module (drive axle and vehicle longitudinal dynamic model) [16–18], as shown in Figure 1.

2.1. The Transmission Input Power Module. The coworking output characteristics of the diesel engine and the torque converter (TC) determine the input power of the transmission. The output torque of the diesel engine T_E is related to its rotational speed ω_E and throttle opening θ and acts on the converter pump as follows:

$$T_E(\omega_E, \theta) = T_P + J_P \dot{\omega}_P, \tag{1}$$

where T_P is the pump torque, J_P is the equivalent inertia of the turbine, and ω_P is the pump speed.

The dimensionless characteristics of the torque converter (including the pump torque coefficient λ_P , TC torque ratio K_{TC}, speed ratio i_{TC}, and efficiency η_{TC}) are used to describe their dynamic equation [19] as follows:

$$\begin{cases} T_P = \lambda_P \rho_{\mathrm{TC}} g D_{\mathrm{TC}}^5 \omega_P^2, \\ T_T = K_{\mathrm{TC}} T_P, \\ \omega_T = i_{\mathrm{TC}} \omega_P, \\ P_T = T_T \omega_T = \eta_{\mathrm{TC}} P_P = K_{\mathrm{TC}} i_{\mathrm{TC}} T_P \omega_P, \end{cases} \tag{2}$$

where ρ_{TC} is the fluid density of the torque converter, D_{TC} is the effective diameter of the torque converter, T_T is the turbine torque, ω_T is the turbine speed, and P_T and P_P are the power of the turbine and pump.

2.2. Wet Clutch Pressure Control Module. Using Stribeck friction models (shown in Figure 2), the clutch friction working mode switches among "in motion ①", "captured and accelerating ②," and "captured and static ③" [20, 21], as shown in Figure 3.

(1) When the relative speed of the clutch $|\triangle\omega|$ is greater than a threshold $\triangle\omega_{\mathrm{tol}}$, the clutch is the "in motion" mode, and the friction torque T_f is the same as the dynamic torque T_d which is given as follows:

$$\begin{aligned} T_f = T_d &= \mathrm{sign}(\Delta\omega) f(\Delta\omega) \mathrm{SRNp} \\ &= \mathrm{sign}(\Delta\omega) f(\Delta\omega) k_d p, \end{aligned} \tag{3}$$

where $f(\Delta\omega) = 0.06 + 0.04e^{(-0.36\Delta\omega)}$ is the friction factor for the copper-based surface and S, R, N, and p are equivalent area, equivalent radius, number of friction pairs, and clutch pressure, respectively. Constants can be summarized as a pressure proportional coefficient $k_d = \mathrm{SRN}$.

(2) When the clutch relative speed $|\triangle\omega|$ is less than the threshold $\triangle\omega_{\mathrm{tol}}$ and the required torque T_{tp} is greater than the dynamic torque T_d, the clutch is in the "captured and accelerating" mode, and the friction torque T_f is the same as the dynamic torque T_d.

(3) When the clutch relative speed $|\triangle\omega|$ is less than the threshold $\triangle\omega_{\mathrm{tol}}$ and the required torque T_{tp} is less than the dynamic torque T_d, the clutch is in the "captured and static" mode, and the friction torque T_f is the same as the required torque T_{tp}.

2.3. Planetary Gear Set Module. In this study, 1st gear to 2nd gear upshift is chosen as the example of an AT shifting process for heavy-duty mining trucks. In the first gear, the clutch CS is engaged to connect the sun gear S_1 to the carrier C_1 of the first planetary gear set P_1 at the same speed. The torque is input from the turbine and output from the ring R_1 of P_1. When the transmission control unit (TCU) issues an upshift command, CS is disengaged by releasing pressure and the on-coming brake BS is engaged gradually. It finally fixes S_1 to the transmission housing to stop its movement and enters the second gear state. With brake BL keeping engaged during the first and second gear, the ring R_3 of the

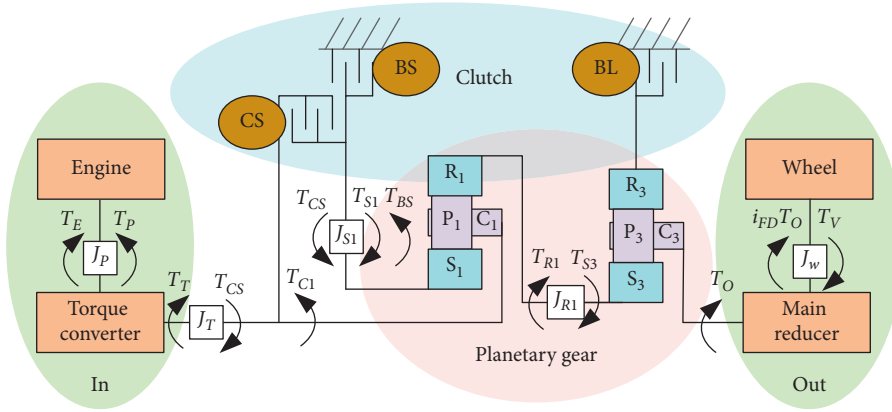

FIGURE 1: Simplified dynamic model of the powertrain consisting of engine, torque converter, two planetary gear sets (P_1 and P_3), clutches (CS, BS, and BL), and vehicle.

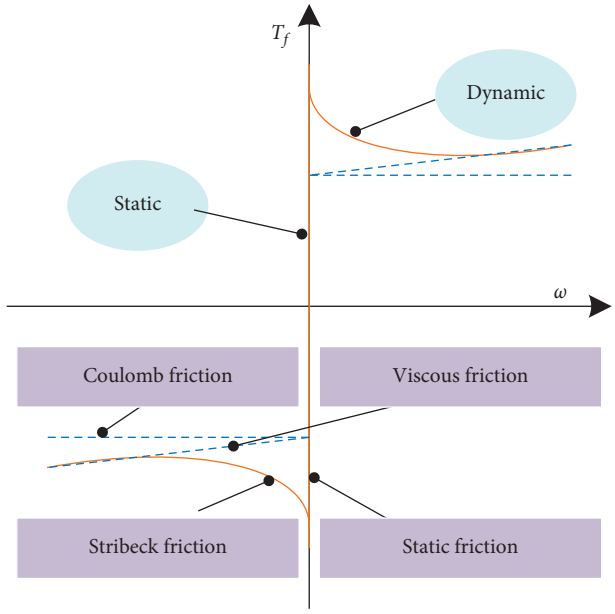

FIGURE 2: Stribeck friction model.

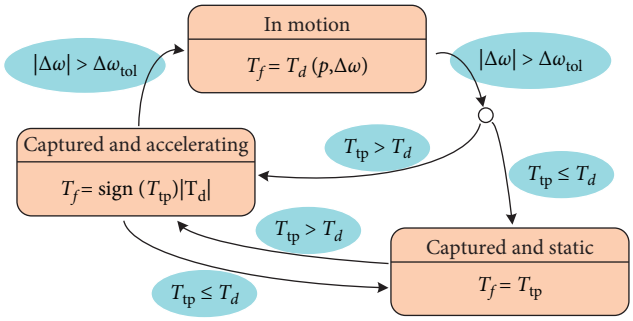

FIGURE 3: Clutch friction working modes and switching according to different transmitted torques and relative speeds of clutches.

3rd planetary gear set P_3 is fixed on the transmission housing, while the torque is transferred from the carrier C_3 to the transmission output shaft. At all time, the planetary row P_3 can be regarded as a reducer with the speed ratio i_{p3}.

By analyzing the transmission input shaft (torque converter turbine shaft), the sun shaft and ring shaft of P_1, and the transmission output shaft, the dynamic equations of the gearbox can be written as follows:

$$\begin{cases} T_T + T_{CS} - T_{C1} = J_T \dot{\omega}_T, \\ T_{S1} - T_{CS} - T_{BS} = J_{S1} \dot{\omega}_{BS}, \\ T_{R1} = k_{p1} T_{S1}, \\ T_{R1} - T_{S3} = J_{R1} \dot{\omega}_{R1}, \\ T_O = i_{p3} T_{S3}, \end{cases} \tag{4}$$

where T_{CS} and T_{BS} are the torques of CS and BS; J_{S1}, J_{R1}, and J_T are the inertias of the sun and ring of P_1 and the transmission input shaft; T_{S1}, T_{C1}, and T_{R1} are the torque of sun, carrier, and ring of P_1, respectively; ω_{BS} is the speed of BS; k_{p1} is the gear ratio of R_1 to S_1; T_{S3} is the torque of S_3; and T_O is the torque of the transmission output shaft.

2.4. The Transmission Output Power Module. The torque output T_O by the AT is finally transmitted to the wheels through the main reducer (speed ratio i_{FD}). For modeling convenience, the longitudinal vehicle model is simplified without considering the vehicle's pitch, yaw, and other motion directions resulting in

$$T_O = \frac{J_w \dot{\omega}_w + T_V}{i_{FD}}, \tag{5}$$

where ω_w is the wheel speed, r_w is the wheel radius, and J_w is the equivalent inertia of wheels. When the heavy-duty mining truck is under the nonbraking condition, the longitudinal resistance torque T_V can be summarized from rolling, air, and climbing resistance as follows:

$$T_V = r_w \left(\mathrm{Mgf}_{\mathrm{roll}} + \frac{C_D S_V}{21.15} v_V^2 + \mathrm{Mg} \sin \alpha \right), \tag{6}$$

where r_w is the radius of the wheel, M is the full load mass, f_{roll} is the rolling resistance coefficient, C_D is the air resistance coefficient, S_V is the windward area, v_V is the vehicle speed, and α is the road slope, respectively.

3. LQR Controller Design

The whole shifting process of the heavy-duty mining truck shift can be divided into four stages, which are rapid draining oil (preshift phase), torque phase, inertia phase, and rapid boosting oil (postshift phase) as shown in Figure 4. The preshift phase ($t_1 \sim t_2$) and postshift phase ($t_4 \sim t_5$) are designed for eliminating the gap between the clutch plates and hoisting transmission capacity, respectively. In the torque phase, the 1st gear speed ratio is still maintained and torque is transferred from CS to BS. At the end of the torque phase, if $T_{CS}(t_3) > 0$, this forward torque will cause shift shock; otherwise, if $T_{CS}(t_3) < 0$, this negative torque will cause power loss. Therefore, in order to make T_{CS} equal to zero, BS should be able to undertake the transmission of output torque independently:

$$T_{BS}(t_3) = \frac{1}{k_{p1}} T_T. \tag{7}$$

Open-loop control is adopted in preshift, postshift, and torque phases because there is no change in the clutch speed [22–24]. However, torque and speed change drastically, last longer, and will produce greater shift jerk and clutch friction loss in the inertial phase, which is why the method based on the LQR is used for this key phase in this paper.

3.1. Establishment of State-Space Model. The turbine speed ω_T, clutch speed ω_{BS}, and clutch pressure p_{BS} of on-coming brake BS are selected as the state variables of the shifting process model:

$$x = \begin{bmatrix} \omega_T & \omega_{BS} & p_{BS} \end{bmatrix}^T. \tag{8}$$

The change rate of p_B is selected as the control variable because it is related to the shift jerk and friction loss of the clutch:

$$u = \frac{\mathrm{d}p_{BS}}{\mathrm{d}t}. \tag{9}$$

From the gearbox dynamic equation, the clutch pressure control equation, and transmission power input and output equations (1)–(6), the powertrain dynamic model can be derived as follows:

$$\begin{aligned} \dot{\omega}_T &= \frac{D_{22}K_{TC}}{D_{24}}\omega_T + \frac{D_{12}D_{23}}{D_{24}}p_{BS} \\ &\quad + \frac{(D_{12}D_{14} - D_{13}D_{22})T_L - D_{22}T_T}{D_{24}}, \\ \dot{\omega}_{BS} &= \frac{D_{12}K_{TC}}{D_{24}}\omega_T + \frac{-D_{11}D_{23}}{D_{24}}p_{BS} \\ &\quad + \frac{(D_{11}D_{14} + D_{13}D_{12})T_L + D_{12}T_T}{D_{24}}, \\ \dot{p}_{BS} &= \frac{\mathrm{d}p_{BS}}{\mathrm{d}t}, \end{aligned} \tag{10}$$

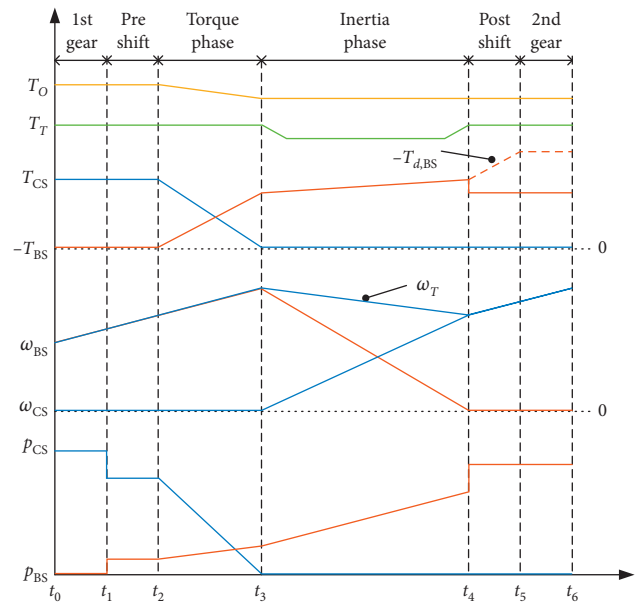

Figure 4: Shifting process with four phases.

where $D_{11} = J_w(1 + k_{p1})^2/k_{p1}^2 i_{p3}^2 + J_T$, $D_{12} = J_w 1 + k_{p1}/k_{p1}^2 i_{p3}^2$, $D_{13} = -1 + k_{p1}/k_{p1}^2 i_{p3}$, $D_{14} = -1/k_{p1} i_{p3}$, $D_{21} = -D_{12}$, $D_{22} = -(J_w 1/k_{p1}^2 i_{p3}^2 + J_{S1})$, $D_{23} = f(\Delta\omega_{BS})k_d$, and $D_{24} = -D_{12}^2 - D_{11}D_{22}$.

The equation of the state-space model in the inertia phase can be written as follows:

$$\dot{x} = Ax + Bu + \Gamma, \tag{11}$$

where $A = \begin{bmatrix} D_{22}K_{TC}/D_{24} & 0 & D_{12}D_{23}/D_{24} \\ D_{12}K_{TC}/D_{24} & 0 & -D_{11}D_{23}/D_{24} \\ 0 & 0 & 0 \end{bmatrix}$, $B = \begin{bmatrix} 0 \\ 0 \\ 1 \end{bmatrix}$, and $\Gamma = \begin{bmatrix} (D_{12}D_{14} - D_{13}D_{22})T_L - D_{22}T_T/D_{24} \\ (D_{11}D_{14} + D_{13}D_{12})T_L + D_{12}T_T/D_{24} \\ 0 \end{bmatrix}$.

3.2. Problem State and the Quadratic Cost Function Definition. The shifting process is not completed instantaneously, and a shifting shock is inevitable. To achieve a smooth shift with a low dynamic load of the system, the vehicle jerk, which is the derivative of acceleration w.r.t. time, should be under control. During the 1-2 upshift process, it can be derived from equations (4) and (5) as follows:

$$\begin{aligned} j = \frac{\mathrm{d}a}{\mathrm{d}t} &= r_w \frac{\mathrm{d}\dot{\omega}_w}{\mathrm{d}t} = \frac{r_w i_{FD} \mathrm{d}T_O}{J_w \mathrm{d}t} \\ &= \frac{r_w i_{FD}}{J_w} k_{p1} i_{p3} \frac{d(f(\Delta\omega_{BS})k_d p_{BS})}{\mathrm{d}t} = c_1 u, \end{aligned} \tag{12}$$

where $c_1 = r_w i_{FD}/J_w k_{p1} i_{p3} f(\Delta\omega_{BS})k_d$.

Although increasing the time of the shift process can reduce the vehicle jerk, this method is not advisable because long-term slipping of the clutch generates friction heat and wear and damages the clutch plates finally. In reference to equation (3), clutch friction loss for BS is modeled as follows:

$$W = \int_0^t \left|T_{f,\mathrm{BS}}\omega_{\mathrm{BS}}\right|\mathrm{d}t = \int_{t_3}^{t_4} \left|f(\omega_{\mathrm{BS}})k_d p_{\mathrm{BS}}\omega_{\mathrm{BS}}\right|\mathrm{d}t = \mathrm{c}_2 \int_{t_3}^{t_4} \left|p_{BS}\omega_{BS}\right|\mathrm{d}t, \tag{13}$$

where $c_2 = f(\Delta\omega_{\mathrm{BS}})k_d$ and t_3 and t_4 represent the start and terminal time of the inertia phase, respectively.

As can be seen from equations (12) and (13), the jerk for the shift in the inertial phase is directly proportional to the control variable, whereas clutch friction loss for BS is proportional to the product of its speed $\omega_{\mathrm{BS}} = x_2$ and pressure $p_{\mathrm{BS}} = x_3$. Therefore, the finite-time linear-quadratic optimization performance index for the shifting inertia phase is shown as follows:

$$J = \frac{1}{2}\int_{t_3}^{t_4}\left(p_{\mathrm{BS}}\omega_{\mathrm{BS}} + ru^2\right)\mathrm{d}t = \frac{1}{2}\int_{t_3}^{t_4}\left(x_2x_3 + ru^2\right)\mathrm{d}t = \frac{1}{2}\int_{t_3}^{t_4}\left(x^TQx + ru^2\right)\mathrm{d}t, \tag{14}$$

where $Q = \begin{bmatrix} 0 & 0 & 0 \\ 0 & 0 & 0.5 \\ 0 & 0.5 & 0 \end{bmatrix}$.

The first term in the integral function represents the clutch friction loss, and the second represents the jerk. By adjusting the comprehensive weight coefficient r (weight coefficient multiplied by a normalized coefficient), the LQR controller can achieve a proper balance between them.

3.3. The Solution of Clutch Pressure Trajectory Based on LQR. According to equations (11) and (14), we introduce the Hamiltonian function [25] as follows:

$$H = \frac{1}{2}\left(x^TQx + ru^2\right) + \lambda(t)^T(Ax + Bu + \Gamma). \tag{15}$$

It is assumed that the shifting proportional solenoid valve of automatic transmission used in this study has a rapid response [26, 27], and there is no limit to the control variable u. According to the maximum principle, we obtain

$$\frac{\partial H}{\partial u} = ru(t) + B^T\lambda(t) = 0, \tag{16}$$

resulting in the optimal control trajectory

$$u^*(t) = -\frac{B^T\lambda(t)}{r}. \tag{17}$$

The normalized equations are as follows:

$$\dot{x} = \frac{\partial H}{\partial \boldsymbol{\lambda}} = Ax + Bu + \Gamma, \tag{18}$$

$$\dot{\lambda}(t) = -\frac{\partial H}{\partial x} = -Qx - A^T\lambda(t). \tag{19}$$

By substituting equation (17) into (18), we obtain

$$\dot{x}(t) = Ax(t) - \frac{BB^T\lambda(t)}{r} + \Gamma. \tag{20}$$

At the end of the inertial phase, clutch BS speed is zero so that terminal constraint function

$$g_T[x(t_4), t_4] = x_2(t_4) = 0. \tag{21}$$

Here, we obtain

$$\lambda(t_4) = \begin{bmatrix}\lambda_1 \\ \lambda_2 \\ \lambda_3\end{bmatrix} = \mu\frac{\partial g_T[x(t_4), t_4]}{\partial x(t_4)} = \begin{bmatrix}0 \\ \mu \\ 0\end{bmatrix}, \tag{22}$$

where μ is the undetermined Lagrange multiplier. Due to the interference matrix Γ, the solution of the conventional LQR, which is letting $\lambda(t) = P(t)x(t)$, cannot be used. Here, we set

$$\lambda(t) = P(t)x(t) + M(t)\mu + h(t), \tag{23}$$

$$g_T = K(t)x(t) + L(t)\mu + \eta(t). \tag{24}$$

According to equations (22), (23), and (24), we obtain

$$P(t_4) = \begin{bmatrix}0 & 0 & 0 \\ 0 & 0 & 0 \\ 0 & 0 & 0\end{bmatrix}, M(t_4) = \begin{bmatrix}0 \\ 1 \\ 0\end{bmatrix}, h(t_4) = \begin{bmatrix}0 \\ 0 \\ 0\end{bmatrix}, \tag{25}$$

$$K(t_4) = \begin{bmatrix}0 & 1 & 0\end{bmatrix}, L(t_4) = 0, \eta(t_4) = 0.$$

Substitution of equation (23) into (19) yields

$$\dot{\lambda}(t) = \left[-Q - A^TP(t)\right]x(t) - A^TM(t)\mu - A^Th(t). \tag{26}$$

Substituting equations (20) and (23) into the derivative of equation (23), we obtain affirmatively

$$\begin{aligned}\dot{\lambda}(t) &= \dot{P}(t)x(t) + P(t)\dot{x}(t) + \dot{M}(t)\mu + \dot{h}(t) \\ &= \left[\dot{P}(t) + P(t)A - \frac{P(t)\mathrm{BB}^TP(t)}{r}\right]x(t) \\ &\quad + \left[\dot{M}(t) - \frac{P(t)BB^TM(t)}{r}\right]\mu \\ &\quad - \frac{P(t)\mathrm{BB}^T}{r}h(t) + P(t)\Gamma + \dot{h}(t).\end{aligned} \tag{27}$$

Comparing equations (26) and (27) w.r.t $x(t)$, μ, and rest, we obtain

$$\dot{P}(t) = -P(t)A - A^TP(t) + \frac{P(t)\mathrm{BB}^TP(t)}{r} - Q, \tag{28}$$

$$\dot{M}(t) = \left[\frac{P(t)\mathrm{BB}^T}{r} - A^T\right]M(t) \tag{29}$$

$$\dot{h}(t) = \left[\frac{P(t)\mathrm{BB}^T}{r} - A^T\right]h(t) - P(t)\Gamma \tag{30}$$

When the terminal time t_4 is finite, these equations are nonlinear and time varying. Therefore, the differential

equations are replaced by the difference equations, and the value at each step can be calculated singly in the reverse direction with $(-\Delta t)$ as the time interval from equation (25).

Substituting equations (20) and (23) into the time derivative of equation (24) yields the following:

$$\begin{aligned}\dot{g}_T &= \dot{K}(t)x(t) + K(t)\dot{x}(t) + \dot{L}(t)\mu + \dot{\eta}(t)\\ &= \left[\dot{K}(t) + K(t)A - \frac{K(t)\mathrm{BB}^T P(t)}{r}\right]x(t)\left[\dot{L}(t) - \frac{K(t)\mathrm{BB}^T M(t)}{r}\right]\mu\\ &\quad - \frac{K(t)\mathrm{BB}^T h(t)}{r} + K(t)\Gamma + \dot{\eta}(t) = 0.\end{aligned} \tag{31}$$

Equation (31) holds for any $x(t)$ and μ, if

$$\dot{K}(t) = K(t)\left[\frac{\mathrm{BB}^T P(t)}{r} - A\right], \tag{32}$$

$$\dot{L}(t) = \frac{K(t)\mathrm{BB}^T M(t)}{r}, \tag{33}$$

$$\dot{\eta}(t) = K(t)\left[\frac{\mathrm{BB}^T h(t)}{r} - \Gamma\right]. \tag{34}$$

Comparing equation (29) with (32) and $M(t_4)$ with $K(t_4)$ in equation (25) shows

$$K(t) = M^T(t). \tag{35}$$

Then, we substitute the initial value of the system in equation (24):

$$\mu = \frac{g_T(t_3) - K(0)x(0) - \eta(0)}{L(0)}. \tag{36}$$

Finally, the optimal control trajectory in equation (17) is

$$\begin{aligned}u^*(t) &= -\frac{B^T\lambda(t)}{r} = -\frac{B^T}{r}\left[P(t)x(t) + M(t)\mu + h(t)\right]\\ &= -\frac{B^T P(t)}{r}x(t) - \frac{B^T}{r}\left[M(t)\mu + h(t)\right]\\ &= V(t)x(t) + W(t),\end{aligned} \tag{37}$$

where control parameters $V(t) = -B^T P(t)/rx(t)$ and $W(t) = -B^T/r\left[M(t)\mu + h(t)\right]$.

4. Simulation Results and Discussion

The LQR controller model and the model of the powertrain system for the heavy-duty mining truck were built in Matlab/Simulink with the major simulation parameters shown in Table 1. No load without road slope under 50% throttle opening and full load with $\alpha = 6^\circ$ road slope under 100% throttle opening are chosen as the normal condition and the extreme condition, respectively, to test the preset reference trajectory [8] and optimal trajectory under variations of comprehensive weight coefficients r.

4.1. Normal Working Condition. The no-load mass of the heavy-duty mining truck in this paper is 30 tons. After starting on a flat road with a 50% throttle opening, the simulation results are shown in Figure 5.

At 1.0 s, where the pressure of CS drops to zero and enters the inertia phase, the BS pressure is controlled by the LQR optimal trajectory described above. The entire shift time is about 0.9 s as shown in Figure 5(a). Although the speed of the turbine shaft and BS begins to decrease, unlike the torque phase, they are no longer the same in the inertial phase because of the clutch CS slipping. When the inertial phase ends, the speed of BS drops to zero, and the turbine speed begins to rise again. Compared with the preset reference trajectory, the optimized speed of BS changes more slowly (as shown in Figure 5(b)). Figure 5(c) shows the trends of BS, CS, and turbine torque in the shifting process. With the rise in BS torque, the torque of CS gradually decreases to zero at the end of the torque phase. The reason for the sudden BS torque change at about 1.5 s (inertia phase ends) is that the clutch friction working mode of BS switches from the "captured and accelerating" mode to the "captured and static" mode, which means the sliding friction becomes static friction.

The result of shifting jerk and clutch friction loss for the LQR controller is compared with that of the preset trajectory controller in Figure 5(d). For $r = 1 * 10^{-6}$, the peak value of the optimized jerk $j_{\max} = 1.33\ \mathrm{m/s^3}$ is slightly smaller than the peak value $j_{\max} = 1.37\ \mathrm{m/s^3}$ before optimization, which satisfies the design requirement of $j \leq \pm 5\ \mathrm{m/s^3}$. At the end of the inertial phase, the loss of clutch friction is $W = 24.7$ kJ after optimization, which is about 26.3% less than $W = 33.5$ kJ for the preset reference controller. By adjusting the weight coefficients to $r = 3.5 * 10^{-6}$, shift jerk drops to $j_{\max} = 1.05\ \mathrm{m/s^3}$, while clutch friction loss increases to $W = 31.3$ kJ, which shows the proposed controller can optimize both objectives.

4.2. Extreme Working Condition. The extreme working conditions of the heavy-duty mining truck studied in this paper are 72 tons at full load and 100% throttle opening on $\alpha = 6^\circ$ road slope. This simulation is for checking the robustness of the LQR controller as shown in Figure 6.

Table 1: Simulation parameters.

Symbol	Value	Unit
J_w	417	$kg \cdot m^2$
J_{S1}	0.31	$kg \cdot m^2$
J_{R1}	0.68	$kg \cdot m^2$
J_P	2	$kg \cdot m^2$
k_{p1}	2	—
i_{p3}	2.67	—
k_d	0.04752	—
i_{FD}	22.4	—
r_w	0.97	m
J_T	2	$kg \cdot m^2$
M	72000	kg
f_{roll}	0.03	—
C_D	0.8	—
S_V	15	m^3

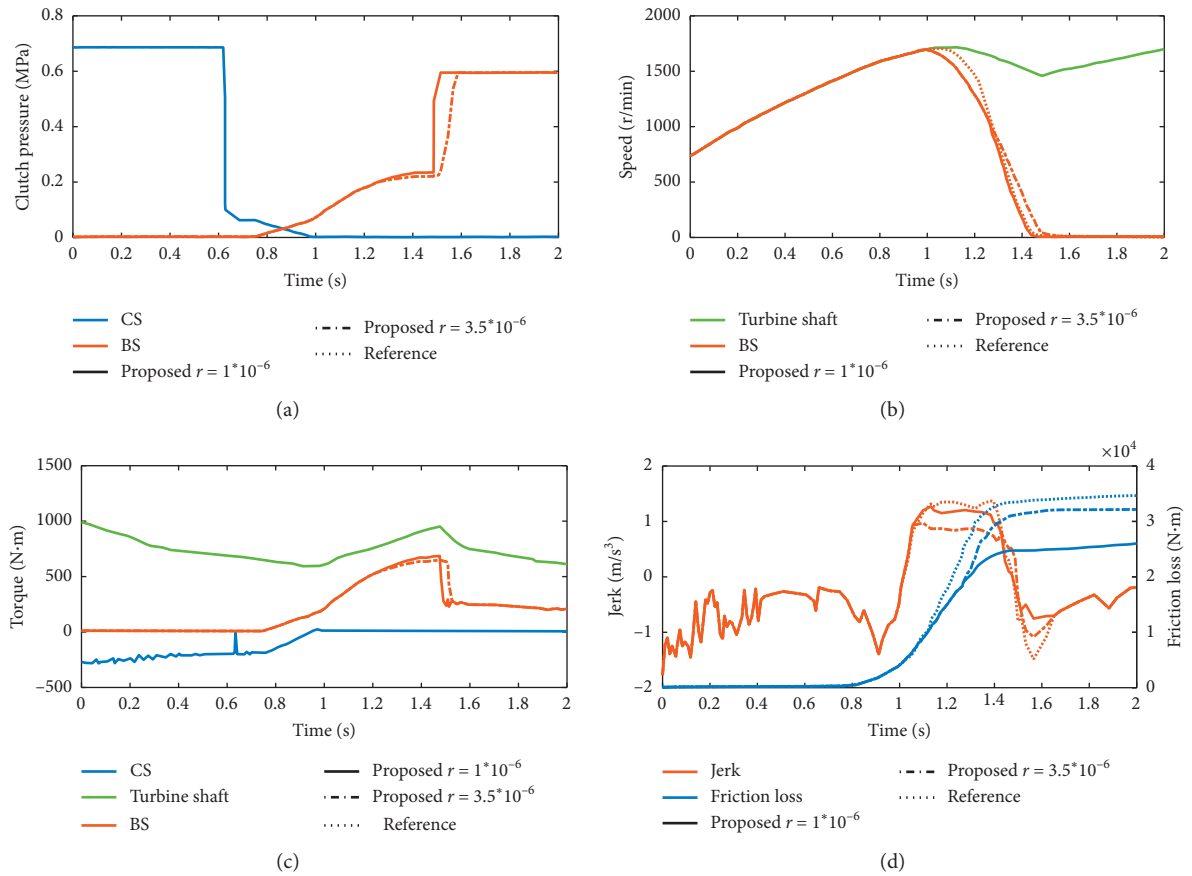

Figure 5: Simulation result with mass $m = 30t$, throttle opening $\theta = 50\%$, and road slope $\alpha = 0°$.

Due to the small acceleration of the vehicle under this condition, the required shifting speed is reached later, starting from 1.3 s and ending at 2.1 s. Compared with normal conditions, the speed and torque of CS, BS, and other transmission components are at higher values. The peak speed of BS exceeds 1700 r/min and the torque reaches 1000 Nm as shown in Figures 6(a)–6(c). In Figure 6(d), it can be seen that after the LQR controller optimizes the clutch pressure, the peak value of the jerk is $j_{max} = 1.97\ m/s^3$ and the final value of clutch friction loss is $W = 42.3$ kJ at the weight coefficient $r = 2.85 * 10^{-6}$, which are less than $j_{max} = 2.33\ m/s^3$ and $W = 52.2$ kJ before optimization, respectively. Under different working conditions, the comparison results of the LQR controller with the reference trajectory controller are shown in Table 2.

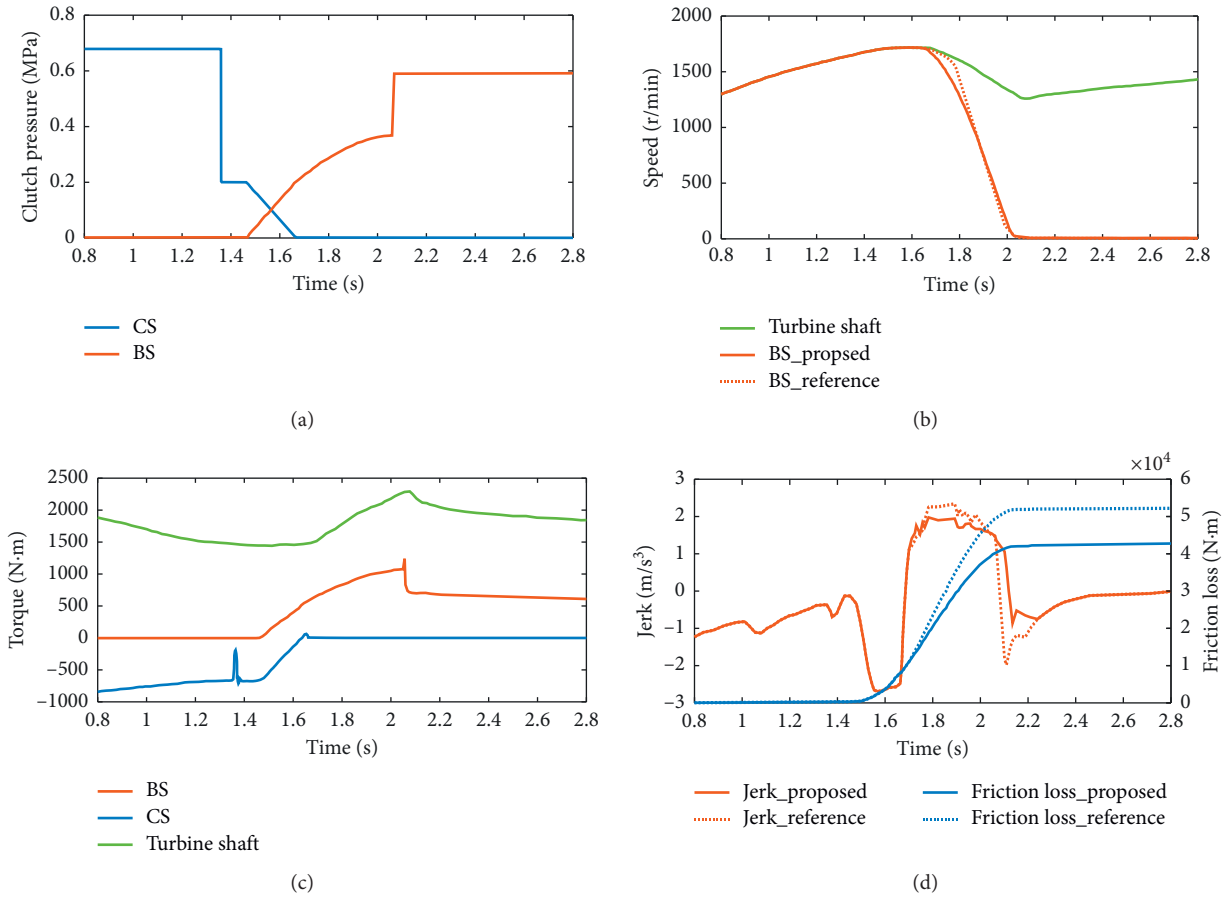

Figure 6: Simulation result with mass $m = 72t$, throttle opening $\theta = 100\%$, road slope $\alpha = 6^\circ$, and comprehensive weight coefficient $r = 2.85 * 10^{-6}$.

Table 2: Comparison results of the LQR controller with the reference trajectory controller under different conditions.

Condition	Controller	j_{max} (m/s^3)	Jerk improve	W (kJ)	Clutch energy loss improve
Normal	Preset reference	1.37	—	33.5	—
	LQR ($r = 1 * 10^{-6}$)	1.33	2.9%	24.7	26.3%
	LQR ($r = 3.5 * 10^{-6}$)	1.05	23.4%	31.3	6.7%
Extreme	Preset reference	2.33	—	52.2	—
	LQR ($r = 2.85 * 10^{-6}$)	1.97	15.5%	42.3	19.0%

5. Conclusions

This paper proposes a clutch pressure control method by linear-quadratic optimization for the inertia phase of an AT shifting process for a heavy-duty mining truck. The powertrain system model and the LQR controller model are built in Matlab/Simulink. The results show that the LQR optimized clutch pressure control trajectory can reduce the jerk and the clutch friction loss for both normal and extreme working conditions. Compared with the preset reference trajectory, their maximum value can drop by 23.4% for jerk and by 26.3% for clutch energy loss under the normal working condition and $j_{max} = 1.97\,\text{m/s}^3$ and $W = 42.3\,\text{kJ}$ at extreme conditions, which indicates that the optimization method results in effective and robust control.

Data Availability

The data used to support the findings of this study are available from the corresponding author upon request.

Conflicts of Interest

The authors declare no potential conflicts of interest with respect to research, authorship, and/or publication of this article.

Acknowledgments

This work was supported by the National Natural Science Foundation of China (grant no. 51905031), the Fundamental

Research Funds for the Central University of China (grant no. FRF-TP-18-036A1), and the National Key Research and Development Program of China (grant no. 2018YFC0604402).

References

[1] P. Dong, Y. Liu, P. Tenberge, and X. Xu, "Design and analysis of a novel multi-speed automatic transmission with four degrees-of-freedom," *Mechanism and Machine Theory*, vol. 108, pp. 83–96, 2017.

[2] Y. Zhang and W. Ma, "Shift control system of heavy-duty vehicle automatic transmission," *Journal of Networks*, vol. 8, no. 12, 2013.

[3] F. Meng, H. Zhang, D. Cao, and H. Chen, "System modeling and pressure control of a clutch actuator for heavy-duty automatic transmission systems," *IEEE Transactions on Vehicular Technology*, vol. 65, no. 7, pp. 4865–4874, 2016.

[4] X. Zhao, W. Zhang, Y. Feng, and Y. Yang, "Optimizing gear shifting strategy for off-road vehicle with dynamic programming," *Mathematical Problems in Engineering*, vol. 2014, Article ID 642949, 9 pages, 2014.

[5] Y. Cheng, P. Dong, S. Yang, and X. Xu, "Virtual clutch controller for clutch-to-clutch shifts in planetary-type Automatic transmission," *Mathematical Problems in Engineering*, vol. 2015, Article ID 213162, 16 pages, 2015.

[6] V. Ranogajec, J. Deur, V. Ivanović, and H. E. Tseng, "Multi-objective parameter optimization of control profiles for automatic transmission double-transition shifts," *Control Engineering Practice*, vol. 93, Article ID 104183, 2019.

[7] J.-Y. Oh, J.-Y. Park, J.-W. Cho, J.-G. Kim, J.-H. Kim, and G.-H. Lee, "Influence of a clutch control current profile to improve shift quality for a wheel loader automatic transmission," *International Journal of Precision Engineering and Manufacturing*, vol. 18, no. 2, pp. 211–219, 2017.

[8] F. Meng, G. Tao, T. Zhang, Y. Hu, and P. Geng, "Optimal shifting control strategy in inertia phase of an automatic transmission for automotive applications," *Mechanical Systems and Signal Processing*, vol. 60-61, pp. 742–752, 2015.

[9] X. Song and Z. Sun, "Pressure-based clutch control for automotive transmissions using a sliding-mode controller," *IEEE/ASME Transactions on Mechatronics*, vol. 17, no. 3, pp. 534–546, 2012.

[10] K. Sanada, B. Gao, N. Kado, H. Takamatsu, and K. Toriya, "Design of a robust controller for shift control of an automatic transmission," *Proceedings of the Institution of Mechanical Engineers, Part D: Journal of Automobile Engineering*, vol. 226, no. 12, pp. 1577–1584, 2012.

[11] X. Zhao and Z. Li, "Data-driven predictive control applied to gear shifting for heavy-duty vehicles," *Energies*, vol. 11, no. 8, p. 2139, 2018.

[12] A. Wurm and D. Bestle, "Robust design optimization for improving automotive shift quality," *Optimization and Engineering*, vol. 17, no. 2, pp. 421–436, 2016.

[13] C. Lin, S. Sun, P. Walker, and N. Zhang, "Off-line optimization based active control of torsional oscillation for electric vehicle drivetrain," *Applied Sciences*, vol. 7, no. 12, p. 1261, 2017.

[14] B. Gao, Q. Liang, Y. Guo, and H. Chen, "Gear ratio optimization and shift control of 2-speed I-AMT in electric vehicle," *Mechanical Systems and Signal Processing*, vol. 50-51, pp. 615–631, 2015.

[15] G. Li and D. Görges, "Optimal control of the gear shifting process for shift smoothness in dual-clutch transmissions," *Mechanical Systems and Signal Processing*, vol. 103, pp. 23–38, 2018.

[16] H. Hwang and S. Choi, "Dynamic driveline torque estimation during whole gear shift for an automatic transmission," *Mechanism and Machine Theory*, vol. 130, pp. 363–381, 2018.

[17] Y. Lei, K. Liu, Y. Zhang et al., "Adaptive gearshift strategy based on generalized load recognition for automatic transmission vehicles," *Mathematical Problems in Engineering*, vol. 2015, Article ID 614989, 12 pages, 2015.

[18] V. Ranogajec, V. Ivanović, J. Deur, and H. E. Tseng, "Optimization-based assessment of automatic transmission double-transition shift controls," *Control Engineering Practice*, vol. 76, pp. 155–166, 2018.

[19] H. Jin-Oh and K. Lee, "Nonlinear robust control of torque converter clutch slip system for passenger vehicles using advanced torque estimation algorithms," *Vehicle System Dynamics*, vol. 37, no. 3, pp. 175–192, 2002.

[20] H. Jian, W. Wei, H. Li, and Q. Yan, "Optimization of a pressure control valve for high power automatic transmission considering stability," *Mechanical Systems and Signal Processing*, vol. 101, pp. 182–196, 2018.

[21] J. Kim and S. B. Choi, "Design and modeling of a clutch actuator system with self-energizing mechanism," *IEEE/ASME Transactions on Mechatronics*, vol. 16, no. 5, pp. 953–966, 2011.

[22] L. Y. Fu and X. Z. Li, "Research on integrated shift control strategy for automatic transmission," *Applied Mechanics and Materials*, vol. 835, pp. 687–692, 2016.

[23] L. Li, X. Wang, X. Qi, X. Li, D. Cao, and Z. Zhu, "Automatic clutch control based on estimation of resistance torque for AMT," *IEEE/ASME Transactions on Mechatronics*, vol. 21, no. 6, pp. 2682–2693, 2016.

[24] S. Li, C. Wu, and Z. Sun, "Design and implementation of clutch control for automotive transmissions using terminal-sliding-mode control and uncertainty observer," *IEEE Transactions on Vehicular Technology*, vol. 65, no. 4, pp. 1890–1898, 2016.

[25] T. Bubnicki, *Modern Control Theory*, Springer, Berlin, Germany, 2005.

[26] T. Ouyang, G. Huang, S. Li, J. Chen, and N. Chen, "Dynamic modelling and optimal design of a clutch actuator for heavy-duty automatic transmission considering flow force," *Mechanism and Machine Theory*, vol. 145, Article ID 103716, 2020.

[27] T. Ouyang, S. Li, G. Huang, F. Zhou, and N. Chen, "Mathematical modeling and performance prediction of a clutch actuator for heavy-duty automatic transmission vehicles," *Mechanism and Machine Theory*, vol. 136, pp. 190–205, 2019.